LA-UR- 97- 1746

CONF-9510259--3

Approved for public release; distribution is unlimited.

Title: THE STATISTICS OF SINGLE MOLECULE DETECTION: AN OVERVIEW

Author(s): J. Enderlein
D. L. Robbins
W. P. Ambrose
P. M. Goodwin
R. A. Keller

Submitted to: Bioimaging, Proceedings of the International Workshop on Single Molecule Detection
Berlin, Germany
10/4-6/95

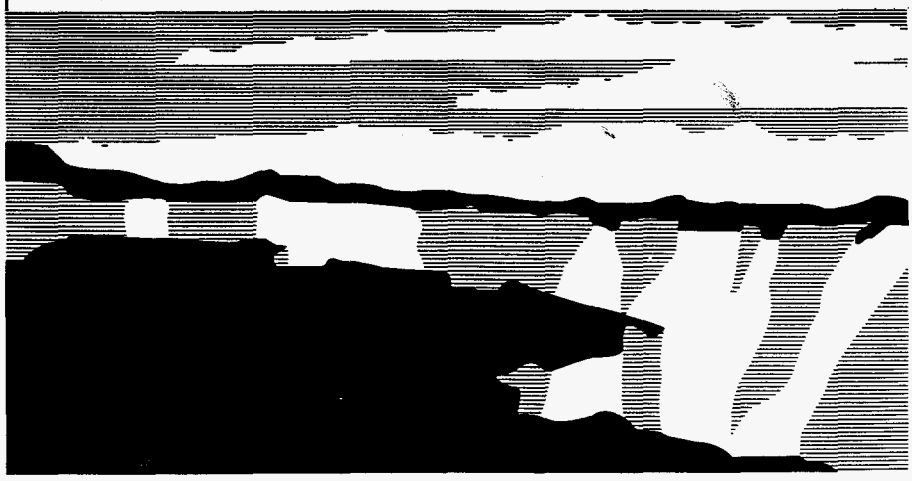

Los Alamos
NATIONAL LABORATORY

Bioimaging

The Statistics of Single Molecule Detection: An Overview

Jörg Enderlein*, David L. Robbins, W. Patrick Ambrose,
Peter M. Goodwin, Richard A. Keller
CST-1, MS M888
Los Alamos National Laboratory
Los Alamos, NM 87545

Abstract

An overview of our recent results in modeling single molecule detection in fluid flow is presented. Our mathematical approach is based on a path integral representation. The model accounts for all experimental details, such as light collection, laser excitation, hydrodynamics and diffusion, and molecular photophysics. Special attention is paid to multiple molecule crossings through the detection volume. Numerical realization of the theory is discussed. Measurements of burst size distributions in single B-phycoerythrin molecule detection experiments are presented and compared with theoretical predictions.

* To whom correspondence should be addressed

1. Introduction

In recent years, the detection and spectroscopy of single molecules has seen tremendous developments. Especially, the detection of single fluorescent molecules in liquids at room temperature has made big advances since the first successful detection of a molecule labeled with multiple fluorophores by Hirschfeld in 1976 [1]. Single molecule detection capabilities have improved to the point where several groups have demonstrated the detection of molecules containing a single fluorophore as the molecule transits a focused laser beam [2-17]. This technique has recently gained much attention in connection with its possible applications to DNA-sequencing [18-[23]], sizing of DNA-fragments [24-26], genetic screening [27,28], diagnostics [29,30], the study of single molecule chemical kinetics [31-34], and the detection of minute amounts of substances [35,36].

The detection of single molecules in liquids at room temperature is a challenging task. This is caused by several effects: the surrounding liquid and possible impurities cause high background signals, diffusion causes molecules to exit or miss the detection volume, and photobleaching limits the overall number of detectable photons from one molecule. Thus, for detecting single molecules under these circumstances and obtaining a maximum amount of information from single molecule experiments, it is desirable to have a sufficiently complete model of the experiment for predictions and comparisons with the measured data. An efficient model allows the experimental conditions to be modified in such a way that one achieves optimal detection results, and to gain information about physical parameters of the studied molecules.

2. Theoretical ingredients

A typical setup of an SMD experiment in fluid flow is shown in Fig.1. Single molecules are eluted from an injection capillary into a surrounding sheath flow that transports them to the detection region defined by focused laser beam and high numerical aperture collection optics. When crossing the laser beam, the single fluorescent molecules produce bursts of fluorescence photons that are detected by an photoelectric detector (e.g.

single photon avalanche diode, multichannel plate, or photomultiplier tube). The resulting photoelectrons are amplified and counted within equally spaced time bins. Subsequently, these raw data can be processed and analyzed on a computer by different algorithms. In the following sections we will collect and consider all the parameters one needs for a full and adequate model description of such a SMD experiment.

2.1. Laser beam profile

In the vast majority of SMD experiments, the optical excitation of the sample is performed by a focused Gaussian laser beam. The intensity profile of such a beam is given by

$$I(x,y,z) = \frac{2P_0}{\pi w^2(y)} \exp\left[-2\frac{x^2+z^2}{w^2(y)}\right], \tag{1}$$

where $w(y)$ is defined by

$$w(y) = w_0\sqrt{1+\left(\frac{\lambda y}{\pi w_0^2}\right)^2}. \tag{2}$$

Here, w_0 denotes the beam waist radius, λ the light wavelength, and P_0 is the total laser power (in photons per time unit). In most cases, the efficient detection region is sufficiently confined near the laser beam waist (due to the fall-off of the optical detection efficiency and the localization of the sample stream), that one can neglect the variation of $w(y)$ along the y-axis and simply replace it by w_0.

2.2. Optical detection efficiency

The optical detection efficiency function, $\eta(\vec{r})$, describes the fraction of the light emitted by an isotropic point source at some object space point $\vec{r}$ that is collected and detected. As was analyzed in [37] by direct wave optical calculations, a simple geometri-

cal optics calculation yields excellent results as long as the involved optical apertures are not too small with respect to the wavelength. Two cases are of special interest: the infinitely long slit aperture, and the rectangular aperture. A principal scheme of the detection optics geometry is shown in Fig.2.

The result for the infinitely long slit aperture of width d is [37]

$$\eta(x,y) = \frac{\eta_0}{\pi(1-\cos\psi)}\left[\arcsin\left(\frac{\sin\theta}{\sin\psi}\right) - \cos\psi \cdot \arctan\left(\frac{\cos\psi\sin\theta}{\sqrt{\sin^2\psi - \sin^2\theta}}\right)\right]_{\theta_{min}}^{\theta_{max}}, \tag{3}$$

where η_0 is the maximum value of the optical collection efficiency, $\psi = \arcsin(\mathrm{NA}/n)$ is the half angle of the cone of light collected by the objective (NA being the numerical aperture and n the refractive index in object space), and the following abbreviations were used:

$$\begin{aligned} \theta_{\min} &= \max\left(-\arctan\left(\frac{d/(2M)+y}{|x|}\right), -\psi\right), \\ \theta_{\max} &= \min\left(\arctan\left(\frac{d/(2M)-y}{|x|}\right), \psi\right), \end{aligned} \tag{4}$$

with M denoting the magnification of the light collecting objective provided that $\theta_{\min} < \theta_{\max}$. If $\theta_{\min} > \theta_{\max}$, then $\eta(x,y)$ is equal to zero. A typical profile of $\eta(x,y)$ is shown in Fig.3.

The result for a rectangular slit of width d and length l is more complicated [37],

$$\eta(x,y,z) = \frac{1}{2\pi(1-\cos\psi)}\int_{v_{min}}^{v_{max}} dv \frac{|x|}{x^2+(v-y)^2}\left[\frac{w-z}{\sqrt{x^2+(v-y)^2+(w-z)^2}}\right]_{w_{min}(v)}^{w_{max}(v)}, \tag{5}$$

where the additional abbreviations

$$
\begin{aligned}
v_{\min} &= \max\left(-d/(2M),\, y-|x|\tan\psi\right)\\
v_{\max} &= \min\left(d/(2M),\, y+|x|\tan\psi\right)\\
w_{\min}(v) &= \max\left(-h/(2M),\, z-\sqrt{x^2\tan^2\psi-(v-y)^2}\right)\\
w_{\max}(v) &= \min\left(h/(2M),\, z+\sqrt{x^2\tan^2\psi-(v-y)^2}\right),
\end{aligned}
\tag{6}
$$

were used, and again provided that $v_{\max} > v_{\min}$ and $w_{\max}(v) > w_{\min}(v)$, otherwise η is zero. It should be mentioned that the integral in Eq.(5) can not be solved analytically and has to be calculated numerically.

2.3. Hydrodynamics and diffusion

In describing the motion of the molecules through the experimental system, two different processes have to be considered: the hydrodynamic flow of the solvent, and the diffusion of single molecules in the solution. In a typical experimental setup as shown in Fig.1, single molecules are eluted from a small injection capillary into the circumflowing sheath flow, which transports them to the detection region. At the injection point into the sheath flow, the velocity of the sample stream can be considered as nearly equal to zero (usually the sheath flow velocity is much larger than the velocity of the sample stream injected through the injection capillary). After injection, the sample stream containing the molecules will be accelerated until a final stationary flow profile is reached. The correct description of the hydrodynamics of the sample stream is rather complicated [38].

Usually the sample stream diameter is sufficiently small compared with the width of the sheath flow channel that one can completely neglect any velocity profile effects over the sample stream diameter. For describing the acceleration of the sample stream after injection, we used in our recent work [39,40] a rather simple idea; we assumed that the acceleration of the sample stream is proportional to the difference between its final stationary velocity v_∞ (given by the peak velocity of the corresponding Poiseuille flow) and its actual velocity at time t, $v(t)$. This yields the following relations between velocity $v(t)$, coordinate $z(t)$, and time t after injection:

$$v(t) = v_\infty\left[1 - \exp(-\kappa t)\right]$$
$$\frac{z(t) - z_{\text{inj}}}{v_\infty} = t - \frac{1}{\kappa}\left[1 - \exp(-\kappa t)\right], \tag{7}$$

where κ is an empirical acceleration parameter.

Two more peculiarities of the injection process have to be taken into account: First, the injection capillary axis can have a lateral shift $\{x_s, y_s\}$ with respect to the crossing point of the laser beam and collection optics axes. Second, the injection of single molecules is not restricted to a point, but will occur over some area of the injection capillary opening. It is convenient to assume that this area is a disk of radius R, and that single molecules are injected uniformly over this area.

Using Eq.(7), the spatial distribution probability of a single molecule at any time t after injection can be given as (no velocity profile effects included)

$$p(\vec{r}, t) = \frac{1}{(4\pi Dt)^{3/2}} \int_0^R \frac{dr}{\pi R^2} r \int_0^{2\pi} d\phi$$
$$\exp\left[-\frac{\left(x - x_s - r\cos\phi\right)^2 + \left(y - y_s - r\sin\phi\right)^2 - \left(z - z(t) + z_{\text{inj}}\right)^2}{4Dt}\right]. \tag{8}$$

For our subsequent considerations, it is important to look at the molecule's motion from yet another point of view. For a diffusive trajectory, $\vec{r}(t')$, $0 \le t' \le t$, what is the probability or the relative weight that a molecule will chose this trajectory? As was shown in [39], this probability will be proportional to

$$\exp\left[-\int_0^t dt' \left(\frac{\dot{\vec{r}}(t') - \vec{v}(t')}{4D}\right)^2\right] \tag{9}$$

Thus, the spatial distribution probability can be written in an alternative way:

$$p(\vec{r},t) \propto \int_0^R dr\, r \int_0^{2\pi} d\phi \int_{(\vec{r}_0,0)\to(\vec{r},t)} \mathcal{D}\vec{r}(t') \exp\left[-\int_0^t dt' \left(\frac{\dot{\vec{r}}(t') - \vec{v}(t')}{4D} \right)^2 \right], \tag{10}$$

where $\vec{r}_0$ is an abbreviation for $\left\{ x_s + r\cos\phi, y_s + r\sin\phi, z_{\text{inj}} \right\}$, and the third integration sign denotes a *path* integration (infinite sum over paths, see e.g. [41,42]) over all possible trajectories in space-time connecting $\vec{r}_0$ at time zero with $\vec{r}$ at time t. It can be shown that the representations Eq.(10) and Eq.(8) are completely equivalent.

2.4. Absorption and fluorescence

For most fluorophores used in SMD, the following photophysical processes are important: absorption of a photon and transition into the first excited state ($S_0 \to S_1$), radiative (fluorescent) or non-radiative return to the ground state ($S_1 \to S_0$), intersystem crossing from the first excited state to the triplet state ($S_1 \to T_1$), return from the triplet state to the ground state ($T_1 \to S_0$), and photobleaching ($S_1 \to \varnothing$). A detailed analysis of this photophysics within the context of single molecule detection was presented in Ref. [43].

Let us first neglect photobleaching, which will be considered in the next subsection. When incorporating the fluorophore's photophysics into a SMD experiment model, a significant simplification nearly always can be made; the time scales of one excitation-fluorescence cycle (~ ns) and of one excitation-triplet state-ground state cycle (~ μs) are typically much faster than the time scale over which the molecule experiences a significant change in illumination intensity due to its motion. Thus, one can apply an adiabatic approximation supposing that at every moment the state populations of a molecule are in equilibrium (the same idea also was applied successfully for handling triplet state effects in fluorescence correlation spectroscopy [44]). Applying this idea, one obtains the following expressions for the populations p_S (excited state) and p_T (triplet state):

$$p_S(\vec{r}) = \frac{\sigma I(\vec{r})\tau}{1+\sigma I(\vec{r})\tau\left(1+k_{isc}\tau_T\right)}$$

$$p_T(\vec{r}) = \frac{\sigma I(\vec{r})k_{isc}\tau\,\tau_T}{1+\sigma I(\vec{r})\tau\left(1+k_{isc}\tau_T\right)}, \tag{11}$$

where σ is the absorption cross section, $I(\vec{r})$ is the (space dependent) light intensity in photons per area per time, τ is the fluorescence lifetime, k_{isc} is the intersystem crossing rate, and τ_T is the triplet state lifetime. The rate of fluorescence is then simply given by $\left(\Phi_f/\tau\right)p_S$, where Φ_f denotes the fluorescence quantum yield. In many cases of practical interest, the intersystem crossing rate is sufficiently small and can be neglected. Moreover, if the excitation light intensity is small enough, one can neglect the denominator in Eq.(11) (no optical saturation).

2.5. Photobleaching

Photobleaching is always present for fluorescent molecules in solution at room temperature. Usually, the photobleaching rate is much slower than the fluorescence decay or triplet-ground state transition rate. The photobleaching rate $V_{bl}(\vec{r})$ is given by

$$V_{bl}(\vec{r}) = k_{2bl}p_S + k_{3bl}p_T, \tag{12}$$

where k_{2bl} and k_{3bl} are the rates for photobleaching occurring in the first excited state and triplet state, respectively. Neglecting optical saturation and other non-linear effects, this equation can be simplified to

$$V_{bl}(\vec{r}) = \Phi_{bl}\sigma I(\vec{r}), \tag{13}$$

where Φ_{bl} is the overall photobleaching quantum yield.

Photobleaching plays an important role in modeling a SMD experiment. To understand the special difficulties connected with photobleaching consider a fixed molecule under constant illumination [39,45]. The time development of the probability that this molecule is not yet photobleached (existence probability) is shown in Fig.4. As long as

no photon is detected this probability decays exponentially with an exponent proportional to the photobleaching quantum yield. When a photon is detected, the detection event provides some information that the molecule was not yet photobleached, causing a jump upwards in the existence probability. Since there is a non-vanishing probability that the detected photon was caused by background, the jump will never bring the existence probability back to unity. In any case, the resulting curve is discontinuous, reflecting the non Markovian character of the whole process (the development of the existence probability does not only depend upon its current value, but upon its complete history).

2.6. Synthesis

We now collect all the pieces together to obtain an expression for the probability $P(N,t_2,t_1)$ to detect a given number of photons within a given interval of time, $\{t_1,t_2\}$. First, we consider the case that only one molecule crosses the detection volume ("pure" single molecule detection). The corresponding probability distribution is denoted by $P_1(N,t_2,t_1)$. The simplest way to do this is to consider the sub-ensemble of all molecules with the same trajectory, $\vec{r}(t)$, through the detection system, and within this sub-ensemble to consider the sub-sub-ensemble of molecules that are all photobleached at the same time t_{bl}. For this sub-sub-ensemble of molecules, the probability $P_1(N,t_2,t_1)$ is simply given by a Poisson distribution with the mean

$$\int_{t_1}^{t_2} dt \left[\theta(t_{bl}-t)V_f[\vec{r}(t)]+V_{bg}\right], \tag{14}$$

where $V_f(\vec{r})$ is the photon detection rate when the molecule is at position $\vec{r}$, V_{bg} is the constant background rate, and $\theta(\cdot)$ denotes Heaviside's step function, being zero for negative values and one for positive. The photon detection rate can be expressed by

$$V_f(\vec{r}) = \eta(\vec{r})\Phi_f \sigma I(\vec{r}) \tag{15}$$

using the same notation as in the above subsections.

Thus, the complete probability distribution $P_1(N, t_2, t_1)$ for all molecules (any trajectory, any photobleaching time) will be a superposition of Poisson distributions,

$$P_1(N, t_2, t_1) = \int_0^\infty d\mathcal{V}_f \, \frac{\mathcal{V}_f^N}{N!} \exp(-\mathcal{V}_f) \cdot \mathcal{P}[\mathcal{V}_f, t_2, t_1], \tag{16}$$

where the weight function $\mathcal{P}[\mathcal{V}_f, t_2, t_1]$ can be given as a path integral over all possible molecule trajectories [39, 40] (compare with Eq.(10)):

$$\begin{aligned}
\mathcal{P}[\mathcal{V}_f, t_2, t_1] = {} & \int \mathcal{D}\,\vec{r}(t) \int_0^T dt_{bl}\, \delta\left[\mathcal{V}_f - \int_{t_1}^{t_2} dt \left[\theta(t_{bl} - t) V_f[\vec{r}(t)] + V_{bg}\right]\right] V_{bl}[\vec{r}(t_{bl})] \cdot \\
& \cdot \exp\left[-\int_0^{t_{bl}} dt \left(\frac{[\dot{\vec{r}}(t) - \vec{v}]^2}{4D} + V_{bl}[\vec{r}(t)]\right)\right] p_0[\vec{r}_0] + \\
& + \int \mathcal{D}\,\vec{r}(t)\, \delta\left[\mathcal{V}_f - \int_{t_1}^{t_2} dt \left[V_f[\vec{r}(t)] + V_{bg}\right]\right] \cdot \\
& \cdot \exp\left[-\int_0^{T} dt \left(\frac{[\dot{\vec{r}}(t) - \vec{v}]^2}{4D} + V_{bl}[\vec{r}(t)]\right)\right] p_0[\vec{r}_0],
\end{aligned} \tag{17}$$

where $\delta[\cdot]$ is a δ-function functional, $p_0(\vec{r}_0)$ is some initial probability distribution of the single molecules at the starting time $t = 0$, and $T > t_2$ is an arbitrary time large enough so that a molecule will have left the detection region with near certainty. The path integration in Eq.(17) runs over all possible paths with arbitrary starting point $\vec{r}_0$ and arbitrary end point. The first term in Eq.(17) accounts for all molecules that photobleach while crossing the laser beam, whereas the second term accounts for all molecules that do not photobleach.

In practical calculations, it is convenient to use as the initial distribution $p_0(\vec{r})$ the distribution of the molecules in a plane perpendicular to the flow direction and upstream of the detection region (where the light intensity is negligibly small), but far enough away from the injection capillary that the sample stream already has reached its final flow ve-

locity v_∞. The corresponding distribution is directly given by Eq.(8), and in Eq.(17) the (generally space dependent) velocity v can be replaced by the constant v_∞.

2.7. Example: Burst size distribution and multiple molecule crossings

The results of the last subsection are directly applicable to the calculation of the burst size distribution (BSD) in a SMD experiment. For pure single molecule crossings it is simply given by Eq.(16) with $t_1 = 0$ and $t_2 = T$. We denote this distribution by $P_1(N)$. One has to take into account that Eq.(16) provides only the distribution for pure single molecule transits, i.e. bursts arising from only single molecules. But for finite concentrations of fluorescent molecules in the sample stream, there exists always a non-vanishing probability that more than only one molecule will traverse the detection volume at the same time. This causes additional peaks in the BSD at higher burst size numbers. A similar effect was reported by Chen and Dovichi when detecting very small numbers of molecules in capillary electrophoresis [36]. There, the fluctuations in the numbers of detected photoelectrons due to the fluctuations of the numbers of molecules in the sampling volume was dubbed "molecular shot noise".

To take into account these multiple molecule crossing effects, one can calculate the BSDs for the different pure k – molecule crossings (k molecules causing an unresolvable single fluorescence burst), and then find the real BSD by a superposition of these k – molecule BSDs.

Under the approximation of a narrow distribution of single molecule burst durations with a mean value τ_b, the k – molecule BSDs can be found from the pure single molecule BSD $P_1(N)$ by simple recursive convolutions:

$$\begin{aligned} P_2(N) &= \sum_{N_1+N_2=N} P_1(N_1)P_1(N_2) \\ P_k(N) &= \sum_{N_1+N_2=N} P_1(N_1)P_{k-1}(N_2), \qquad k>2. \end{aligned} \tag{18}$$

The relative weights w_k of the P_k in the complete BSD are given by

$$w_k = \exp\left(-\frac{2\tau_b}{\tau_m}\right)\left[1-\exp\left(-\frac{\tau_b}{\tau_m}\right)\right]^{k-1}, \tag{19}$$

where τ_m is the mean time between two molecules crossing the detection region ($1/\tau_m$ is the mean injection rate).

3. Numerical considerations

In general, it is impossible to find an analytical expression for $\mathcal{P}\left[\mathcal{V}_f, T, 0\right]$ and thus for $P_1(N,T,0)$. The most convenient numerical method to calculate these functions is by means of a Monte-Carlo simulation. The basic difficulty in calculating Eq.(17) is that the path integral runs over an infinite number of paths. The idea of a Monte-Carlo calculation is to choose these paths randomly, and then to perform the remaining integration exactly. It should be emphasized, that this kind of Monte-Carlo sampling is much more efficient than a straightforward Monte-Carlo sampling, where all the physics (paths, photobleaching, detected fluorescence) is modeled by random processes.

Thus, the course of the calculation is as follows. The time interval $\{0,T\}$ is divided into discrete but sufficiently small time steps, Δt, so that the laser light intensity and detection efficiency that the moving molecule experiences does not change significantly within time Δt. For the discretized times $\{0, \Delta t, 2\Delta t, \ldots, T\}$ and fixed initial position $\vec{r}_0$, a given number of random paths $\{\vec{r}_0, \vec{r}_1, \ldots, \vec{r}_{T/\Delta t}\}$ are generated by means of the probability distribution

$$p(\vec{r}_{k+1} - \vec{r}_k) = \frac{1}{\left[4\pi D\Delta t\right]^{3/2}} \exp\left[-\frac{\left(\vec{r}_{k+1} - \vec{r}_k - \vec{v}\Delta t\right)^2}{4D\Delta t}\right]. \tag{20}$$

For these paths, the integrals occurring in Eq.(17) are calculated numerically by an appropriate integration scheme. For every value of t_{bl} and every occurring positive value of

$$\mathcal{V}_f = \int_0^{\min(T,t_{bl})} dt V_f\left[\vec{r}(t)\right], \tag{21}$$

the corresponding values

$$V_{bl}\left[\vec{r}(t_{bl})\right] \cdot \exp\left[-\int_0^{t_{bl}} dt\left(\frac{\left[\dot{\vec{r}}(t)-\vec{v}\right]^2}{4D} + V_{bl}\left[\vec{r}(t)\right]\right)\right] p_0\left[\vec{r}_0\right] \tag{22}$$

and (for all $t_{bl} > T$)

$$\exp\left[-\int_0^{T} dt\left(\frac{\left[\dot{\vec{r}}(t)-\vec{v}\right]^2}{4D} + V_{bl}\left[\vec{r}(t)\right]\right)\right] p_0\left[\vec{r}_0\right] \tag{23}$$

are added to the final (not yet normalized) result $\mathcal{P}\left[\mathcal{V}_f, T, 0\right]$. When sampling a sufficient large number of paths, one yields an arbitrarily exact distribution function $\mathcal{P}\left[\mathcal{V}_f, T, 0\right]$. After normalizing, one can directly calculate P_1 via Eq.(16).

4. Data analysis

We have found that a Lee filter is an effective method for smoothing the data prior to searching for bursts. A Lee filter of width $2m+1$ is defined as follows. A running mean and variance are calculated using

$$\begin{aligned} \bar{n}_k &= \frac{1}{(2m+1)} \sum_{j=-m}^{m} n_{k+j} \qquad , m < k \le N-m \\ \sigma_k^2 &= \frac{1}{(2m+1)} \sum_{j=-m}^{m} \left(n_{k+j} - \bar{n}_{k+j}\right)^2 \quad , 2m < k \le N-2m, \end{aligned} \tag{24}$$

where N is the total number of data points. The value of k is limited by the window width. The filtered data, $\tilde{n}_k$, are given by:

$$\tilde{n}_k = \bar{n}_k + \left(n_k - \bar{n}_k\right) \frac{\sigma_k^2}{\sigma_k^2 + \sigma_0^2}, \tag{25}$$

where σ_0 is a constant filter parameter. The main action of the Lee filter is preferential smoothing of the photon shot noise in the background, thus facilitating the finding of proper photoelectron bursts. A burst is defined by any continuous number of bins with $\tilde{n}_k > n_{th}$, where n_{th} is a predefined threshold value. We found that the Lee filter works very well if $2m+1$ is of the order of the mean number of time bins per burst, σ_0 is of the order of the mean burst height (mean number of counts per bin in a burst), and n_{th} is above the mean count number of background noise per time bin.

5. Experimental examples

5.1. Experimental set-up and model parameters

In the following we report results of SMD experiments and their comparison with theoretical predictions. All measurements reported in this paper were made on B-phycoerythrin molecules. These macromolecules have very high absorption cross section and unity quantum fluorescence yield, thus being a favorite model system for single molecule detection in fluid flow.

The experimental apparatus used to collect the B-Phycoerythrin data is similar to that previously used for DNA fragment sizing [24-26]. Excitation was accomplished with a continuous wave or a mode locked (200 ps pulse width @ 82 MHz) Ar^- laser operated at 514.5 nm. The output was attenuated with a polarizer / half wave plate assembly and focused to a 20 μm ($1/e^2$ diameter) circular spot at the center of a 250×250 μm^2 square bore sheath flow cuvette (NSG Precision Cell, Inc.). Fluorescence was collected at 90° with a 40 ×, 0.85 NA microscope objective (Nikon Fluor) and spatially filtered with a 400 μm slit located at the image plane of the microscope objective. The probe volume thus defined was approximately 3 pl. Light passing through the slit was spectrally filtered with a 30 nm bandpass filter centered at 575 nm (575DF30 Omega Optical). The filtered light was focused onto the 200×200 μm^2 active area of a photon counting avalanche photodiode (SPCM-200-PQ C.D. 2027, EG&G Optoelectronics Canada) using a 10 × microscope objective.

The sheath fluid was ultra pure water delivered to the flow cell using gravity feed. The sheath volumetric flow rate was adjusted to give transit times through the probe volume in the range of 0.4-6 ms. B-Phycoerythrin dissolved in 1 × Dulbecco's phosphate buffered saline at a concentration of $1.4 \cdot 10^{-10}$ M was forced through a capillary (O.D. 90 μm , I.D. 20 μm , Polymicro Technologies) via a pressure differential. B-Phycoerythrin was eluted from the capillary tip positioned inside the square bore cuvette approximately 100 μm upstream of the probe volume.

Photoelectron pulses from the photodiode were amplified, conditioned with a constant fraction discriminator, and counted with a multichannel scalar (MCS) PC card (Oxford Instruments). The time bin width was chosen to be $50\,\mu\text{sec}$. The raw data were processed by a Lee filter with $m = 5$, $\sigma_0 = 5$, and n_{th} just above the mean background count number.

The following parameter values were used throughout all calculations: diffusion constant $D = 43\,\mu\text{m}^2/\text{sec}$, absorption cross section $\sigma = 5.4 \cdot 10^{-7}\ \mu\text{m}^2$, fluorescence quantum yield $\Phi_f = 0.98$, laser beam waist radius $w_0 = 10\,\mu\text{m}$, width of the slit image in the object space $d = 10\,\mu\text{m}$, maximum detection efficiency $\eta_0 = 1.3 \cdot 10^{-2}$, and distance of the injection point from the laser beam $z_{\text{inj}} = -100\,\mu\text{m}$. The sample stream diameter at the detection volume was determined mainly by the lateral diffusion of the molecules during the time between injection and detection. The time step used in the Monte-Carlo simulation was $\Delta t = 50\,\mu\text{sec}$. The integration time T within the calculations was chosen large enough so that the molecules always passed through the detection region. For every calculation of $\mathrm{P}\left[\mathcal{V}_f, T, 0\right]$, 10^4 paths were sampled. One simulation of a complete burst size distribution took around 5 min on a 586-processor 133-MHz PC. All simulation programs are written with *Matlab* and can be requested from the authors [46].

There remained six unknown parameters which were adjusted: the photobleaching quantum yield Φ_{bl}, the flow velocity v_∞ (assumed to be uniform over the detection region), the position of the sample stream axis x_s, y_s, the hydrodynamically focused sam-

ple stream radius in the absence of diffusion R, and the acceleration parameter κ [39,40]. The acceleration parameter was found to be constant for our set-up and equal to $\kappa = 175\ \mathrm{sec}^{-1}$. We observed that the photobleaching constant was different for cw and pulsed laser excitation.

5.2 Single molecule burst size distribution and burst size broadening

In [39], we presented an analysis of burst size distributions of B-phycoerythrin with low injection rates over a range of sheath flow velocities for cw-excitation. The parameters used in the model calculations were $\Phi_{bl} = 1.4 \cdot 10^{-5}$ and $R = 0.1\ \mu\mathrm{m}$. For every flow velocity, the sample stream displacement was found to be slightly different, due to a readjustment of the detection system between experiments. A typical result of the comparison between experiment and theory is shown in Fig.5. Bursts larger than 250 photoelectrons are due to multiple molecule crossing, which will be accounted for below.

An unexpected result of the model calculation was the fact that the overall width of the BSD is determined mostly by the lateral shift $\{x_s, y_s\}$ of the sample stream. A dramatic change of the BSDs shape can be seen in Fig.6, where the BSD for different displacements are plotted (all remaining parameters the same as Fig.5). It should be noted that jitter of the sample stream position can have a similar effect on the BSD.

5.3 Multiple burst events - molecular noise

In [40], we analyzed SMD experiments with different injection rates, thus dealing specifically with the problem of multiple molecule crossings through the detection volume. These measurements were made using pulsed excitation, resulting in a larger photobleaching quantum yield ($\Phi_{bl} = 6 \cdot 10^{-5}$). In Fig.7, the measured BSDs are shown. In Fig.8, a fit of 7 distributions $P_k(N)$, $1 \le k \le 7$, to the experimental curve with the highest injection rate is shown. On the basis of Eq.(19), the product of the mean (single molecule) burst duration, τ_b, and the average molecule delivery rate, $1/\tau_m$, was determined

for every BSD. The plot of the resulting values against the injection pressure is shown in Fig.9. The linearity of this plot demonstrates the excellent consistency of the theoretical model with the experimental reality.

6. Conclusions

Currently, the weakest point in the theoretical model of SMD in fluid flow is the rather simple assumptions concerning the hydrodynamics of the fluid flow. Future work is required to improve our understanding of this point. Nonetheless, the agreement between experiment and theoretical model is excellent. The developed theoretical approach is very powerful and can be extended to include different generalizations and modifications of the experimental conditions, such as nonlinear photophysics (e.g. multiple photon excitation), or different flow geometries of the sample stream. The path integral approach works well not only for modeling SMD experiments in flow, but also for obtaining autocorrelation functions in fluorescence correlation spectroscopy, as was shown in [47].

There are special cases of data analysis in SMD experiments, where the powerful path integral approach is no longer applicable. Two of them are the calculation of the transit time distribution (distribution of the burst durations), and the calculation of the burst height distribution (distribution of the maximum number of counts per bin per burst).

The calculation of the transit time distribution depends crucially on how a burst duration is defined. As was described in the present paper, one successful way to extract bursts and thus burst durations from the data is the application of a Lee filter. Since this filter involves some arbitrary constants (σ_0, m), it is very difficult to define correct probability distributions of the transit time on a purely theoretical basis. The best one can do is to run a straightforward and simple Monte-Carlo simulation of the whole experiment, using all the details as presented in subsections 2.1-5.

Whereas the transit time distribution is normally of no interest in most applications, the burst height distribution might be quite useful in SMD experiments, where

more than only a single fluorescent molecular species is involved. The reason is, that, in contrast to the BSD, molecular shot noise is only weakly reflected in burst height distributions. If one is interested in distinguishing different molecular species (with different fluorescence strengths) on a single molecule level, then a burst height distribution may be more useful than the BSD. Due to the fact that in calculating a burst height distribution, one asks for a distribution of a *maximum* count number per burst, a closed analytical presentation like Eq.(16,17) will be extremely voluminous. Here again, running a direct Monte-Carlo simulation is the best one can do.

A completely new dimension of data, which we did not consider in the present paper, is offered by measuring not only fluorescence intensities (counts per time bin on a microsecond scale), but also the decay of the fluorescence on a nanosecond time scale. This additional information can e.g. be used to discriminate between different molecular species with different fluorescence decay times. Detailed theoretical analysis of this kind of SMD can be found in [48-50] and [43].

Acknowledgments

JE greatly acknowledges the support of the German Academic Exchange Service, granting him his stay with the Los Alamos National Laboratory. JE thanks also Edgar Klose (GMBU e.V. Berlin) for the great support of his work.

References

1. T. Hirschfeld, Appl. Opt. 15 (1976) 2965.
2. E.B. Shera, N.K. Seitzinger, L.M. Davis, R.A. Keller, and S.A. Soper, Chem. Phys. Lett. 174 (1990) 553.
3. S.A. Soper, E.B. Shera, J.C. Martin, J.H. Jett, J.H. Hahn, H.L. Nutter, and R.A. Keller, Anal. Chem. 63 (1991) 432.
4. S.A. Soper, L.M. Davis, and E.B. Shera, J. Opt. Soc. Am. B 9 (1992) 1761.
5. W.B. Whitten, J.M. Arnold, J.M. Ramsey, and B.V. Bronk, Anal. Chem. 63 (1991) 1027.
6. S.A. Soper, Q.L. Mattingly, and P. Vegunta, Anal. Chem. 65 (1993) 740.
7. C.W. Wilkerson jr., P.M. Goodwin, W.P. Ambrose, J.C. Martin, and R.A. Keller, Appl. Phys. Lett. 62 (1993) 2030.
8. Y.H. Lee, R.G. Maus, B.W. Smith, and J.D. Winefordner, Anal. Chem. 66 (1994) 4142.
9. R. Rigler, J. Widengren, and Ü. Mets, in *Fluorescence Spectroscopy*, edited by O. S. Wolfbeis (Springer, Berlin, 1992) 13.
10. Ü. Mets and R. Rigler, J. Fluores. 4 (1994) 259.
11. S. Nie, D.T. Chiu, and R.N. Zare, Science 266 (1994) 1018.
12. S. Nie, D.T. Chiu, and R.N. Zare, Anal. Chem. 67 (1995) 2849.
13. L.-Q. Li and L.M. Davis, Appl. Opt. 34 (1995) 3208.
14. P.M. Goodwin, R.L. Affleck, W.P. Ambrose, J.H. Jett, M.E. Johnson, J.C. Martin, J.T. Petty, J.A. Schecker, M. Wu, and R.A. Keller, in *Computer Assisted Analytical Spectroscopy*, edited by S.D. Brown, in press (John Wiley and Sons, New York, 1996).
15. M.D. Barnes, W.B. Whitten, J.M. Ramsey, Anal. Chem. 67 (1995) 418A.

16. R.A. Keller, W.P. Ambrose, P.M. Goodwin, J.H. Jett, J.C. Martin, and M. Wu, Appl. Spectrosc. 50 (1996) 12A.

17. P.M. Goodwin, W.P. Ambrose, R.A. Keller, Acc. Chem. Res. 29 (1996) 607.

18. J.H. Jett, R.A. Keller, J.C. Martin, B.L. Marrone, R.K. Moyzis, R.L. Ratliff, N.K. Seitzinger, E.B. Shera, and C.C. Stewart, J. Biomolec. Struct. and Dyn. 7 (1991) 301.

19. J.D. Harding and R.A. Keller, Trends in Biotech. 10 (1992) 55.

20. W.P. Ambrose, P.M. Goodwin, J.H. Jett, M.E. Johnson, J.C. Martin, B.L. Marrone, J.A. Schecker, C.W. Wilkerson, R.A. Keller, A. Haces, P.-J. Shih, and J.D. Harding, Ber. Bunsenges. Phys. Chem. 97 (1993) 1535.

21. P.M. Goodwin, J.A. Schecker, C.W. Wilkerson, M.L. Hammond, W.P. Ambrose, J.H. Jett, J.C. Martin, B.L. Marrone, and R.A. Keller, Proc. SPIE vol. 1891 (1993) 127.

22. P.M. Goodwin, R.L. Affleck, W.P. Ambrose, J.N. Demas, J.H. Jett, J.C. Martin, L.J. Reha-Krantz, D.J. Semin, J.A. Schecker, M. Wu, and R.A. Keller, Exp. Tech. Phys. 41 (1995) 279.

23. P.M. Goodwin, H. Cai, J.H. Jett, S.L. Ishaug-Riley, N.P. Machara, D.J. Semin, Orden A. Van, R.A. Keller, "Application of Single Molecule Detection to DNA Sequencing," Nucleosides and Nucleotides (1996) in press.

24. P.M. Goodwin, M.E. Johnson, J.C. Martin, W.P. Ambrose, B.L. Marrone, J.H. Jett, and R.A. Keller, Nucleic Acids Res. 21 (1993) 803.

25. J.T. Petty, M.E. Johnson, P.M. Goodwin, J.C. Martin, J.H. Jett, and R.A. Keller, Anal. Chem. 67 (1995) 1755.

26. Z. Huang, J.T. Petty, B. O'Quinn, J.L. Longmire, N.C. Brown, J.H. Jett, and R.A. Keller, Nucl. Acids Res. 24 (1996) 4202.

27. A. Castro and E.B. Shera, Anal. Chem. 67 (1995) 3181.

28. A. Castro and E.B. Shera, Appl. Opt. 34 (1995) 3218.

29. M. Eigen and R. Rigler, Proc. Natl. Acad. Sci. USA 91 (1994) 5740.

30. R. Rigler, J. Biotechnol. 41 (1995) 177.

31. Q. Xue and E.S. Yeung, Nature 373 (1995) 681.

32. J. Wang and P. Wolynes, Phys. Rev. Lett. 74 (1995) 4317.

33. M. Wu, P.M. Goodwin, W.P. Ambrose, R.A. Keller, J. Phys. Chem. 100 (1996) 17406.

34. J. Widengren, J. Dapprich, R. Rigler, Chem. Phys. 216 (1997) 417.

35. D.Y. Chen, K. Adelhelm, X.L. Cheng, and N.J. Dovichi, Analyst 119 (1994) 349.

36. D.Y. Chen, N.J. Dovichi, Anal. Chem. 68 (1996) 690.

37. J. Enderlein, W.P. Ambrose, "The optical collection efficiency function in single molecule detection experiments," Appl. Opt. (1997) in press.

38. V. Kachel, H. Fellner-Feldegg, E. Menke, "Hydrodynamic properties of flow cytometry instruments," in: *Flow cytometry and sorting;* Eds.: M.R. Melamed, T. Lindmo, M.L. Mendelsohn; (Wiley-Liss, 1990) 27.

39. J. Enderlein, D.L. Robbins, W.P. Ambrose, P.M. Goodwin, R.A. Keller, "The statistics of single molecule detection," J. Phys. Chem. (1997) in press.

40. J. Enderlein, D.L. Robbins, W.P. Ambrose, R.A. Keller, "Molecular Shot Noise, Burst Size Distributions, and Single Molecule Detection in Fluid Flow," submitted to J. Phys. Chem.

41. R.P. Feynman and A.R. Hibbs, *Quantum mechanics and path integrals* (McGraw-Hill, New York, 1965).

42. H. Kleinert, *Path integral in quantum mechanics, statistics and polymer physics* (2nd. Ed., World Scientific, Singapore, 1994).

43. J. Enderlein, Appl. Opt. 34(3) (1995) 514.

44. J. Widengren, U. Mets, R. Rigler, J. Phys. Chem. 99 (1995) 13368.

45. J. Enderlein, Proc. SPIE. vol.2136 (1994) 226.

46. A *Matlab* program code of the Monte-Carlo sampling can be obtained by sending an e-mail to j.enderlein@tbx.berlinet.de. *Matlab* is a registered trademark by MathWorks Inc.

47. J. Enderlein, Phys. Lett. A 221 (1996) 427.

48. M. Köllner, J. Wolfrum, J. Chem. Phys. Lett. 200 (1992) 199.

49. J. Enderlein, Exp. Tech. Phys. 39 (1991) 479.

50. M. Köllner, Appl. Opt. 32 (1993) 806.

Figures

Fig.1: Sheath flow SMD experimental schematic.

Fig.2: Light collection geometry for a point source located below the center of the image of the slit.

Fig.3: Spatial dependence of the CEF in the x-y-plane for a slit image width of 10 μm, a NA of 0.85, and $n = 1.33$.

Fig.4: Model calculation of the existence probability of a single molecule due to photobleaching. Each arrow indicates the detection of a photon. The photobleaching rate was assumed to be 0.8 per time unit, the ratio of the probability of detecting a background photon to the probability of detecting a fluorescence photon was set to be 0.2 per time unit.

Fig.5: Measured BSD (crosses) and simulation result (solid line) for $v_\infty = 3.5$ mm/sec, $x_s = 3.2$ μm, and $y_s = 1.5$ μm. For comparison, a simulation result with $x_s = 0, y_s = 0$ is shown (dashed line).

Fig.6: Broadening of the burst size distribution with increasing value of x_s ($y_s = 0$). Calculated curves for $x_s = 0$ (narrowest distribution) up to $x_s = 3$ μm (broadest distribution) in steps of 0.5 μm are shown. The laser beam waist radius is $w_0 = 10$ μm.

Fig.7: Measured BSDs for different injection pressures (numbers on the right side in units of mm Hg).

Fig.8: Comparison between measured (circles) and calculated (upper solid line) BSD for the highest injection rate ($p = 200$ mm Hg). In the calculation, the distributions $P_k(N)$ were calculated for $k = 1 \ldots 7$ and fitted to the experimental curve by a least square fit. The different component distributions are shown as solid lines, too.

Fig.9: Linear fit of the determined τ_b/τ_m -values to the injection pressure.

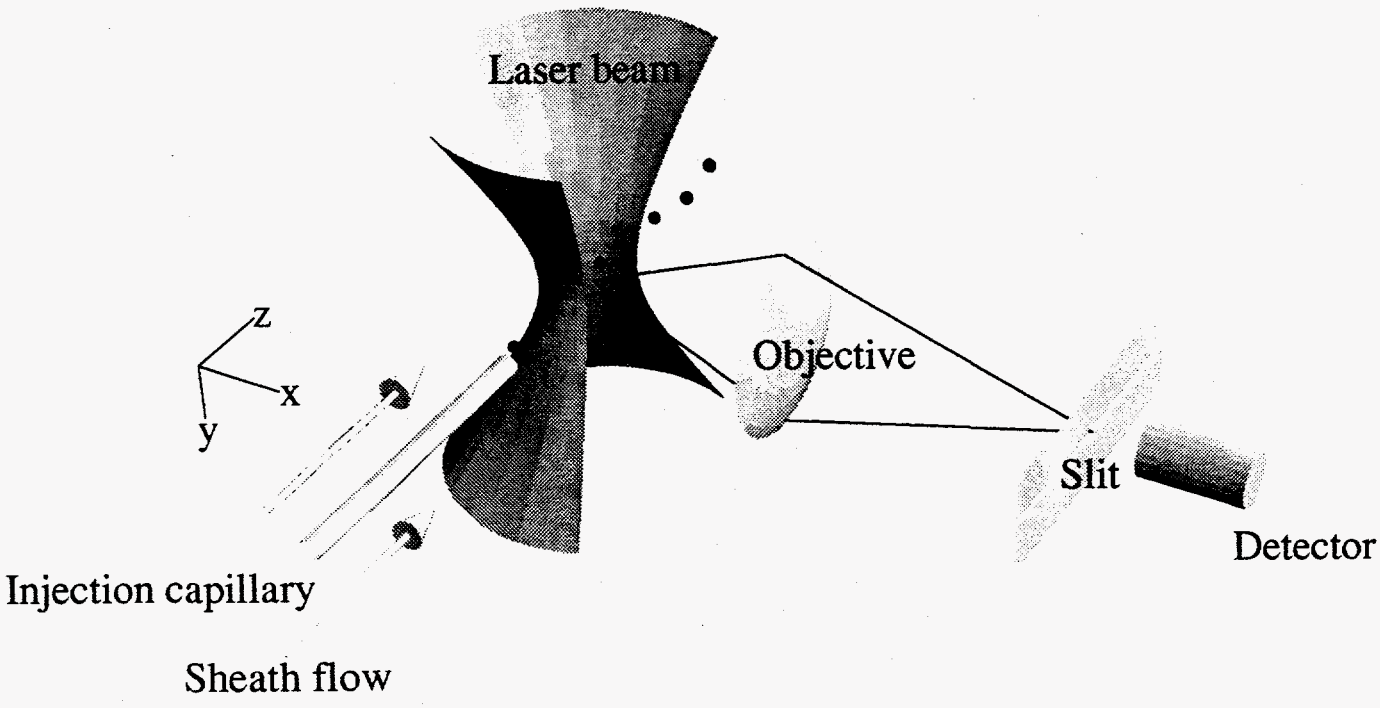
Laser beam
z
x
y
Objective
Slit
Detector
Injection capillary
Sheath flow

Fig. 1

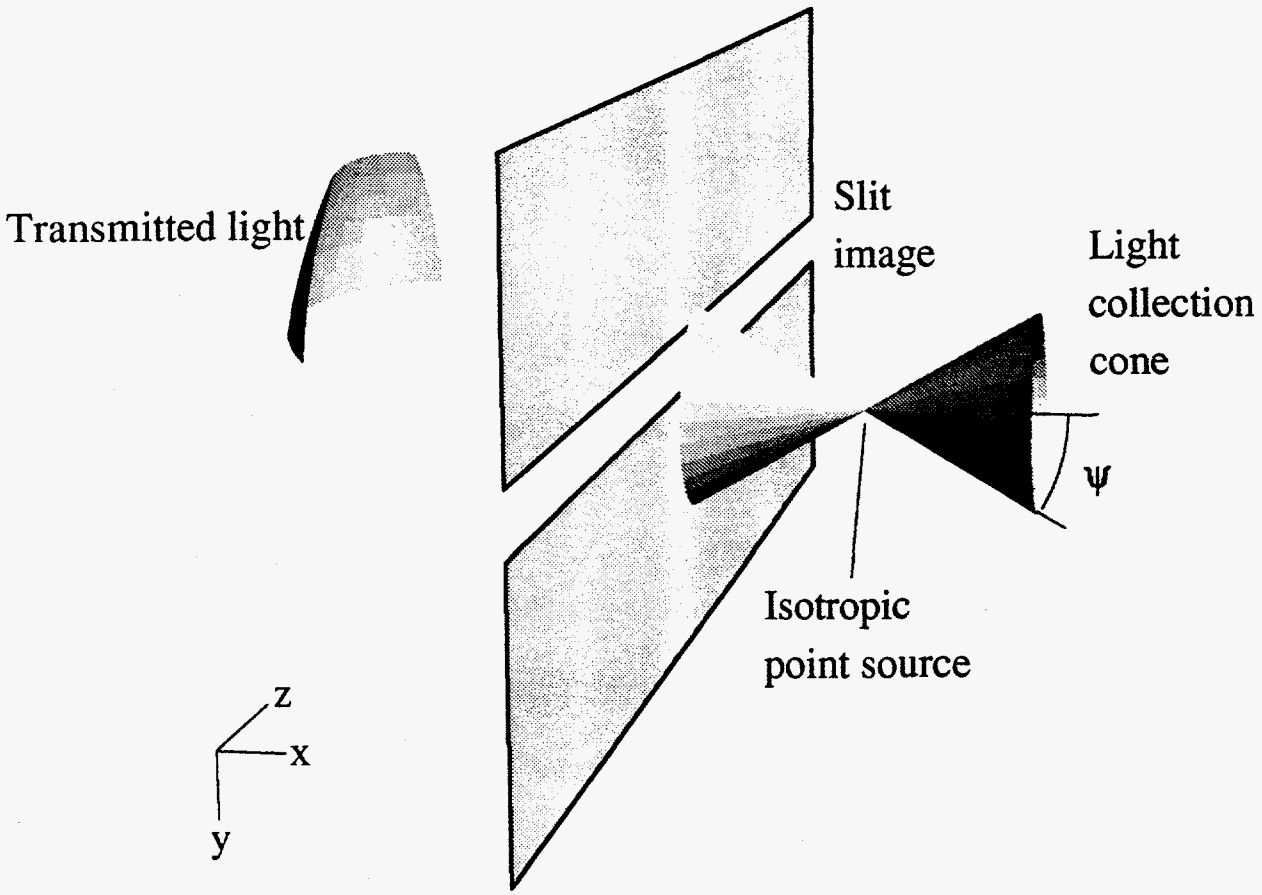
Transmitted light
Slit
image
Light
collection
cone
ψ
Isotropic
point source
z
x
y

Fig. 2

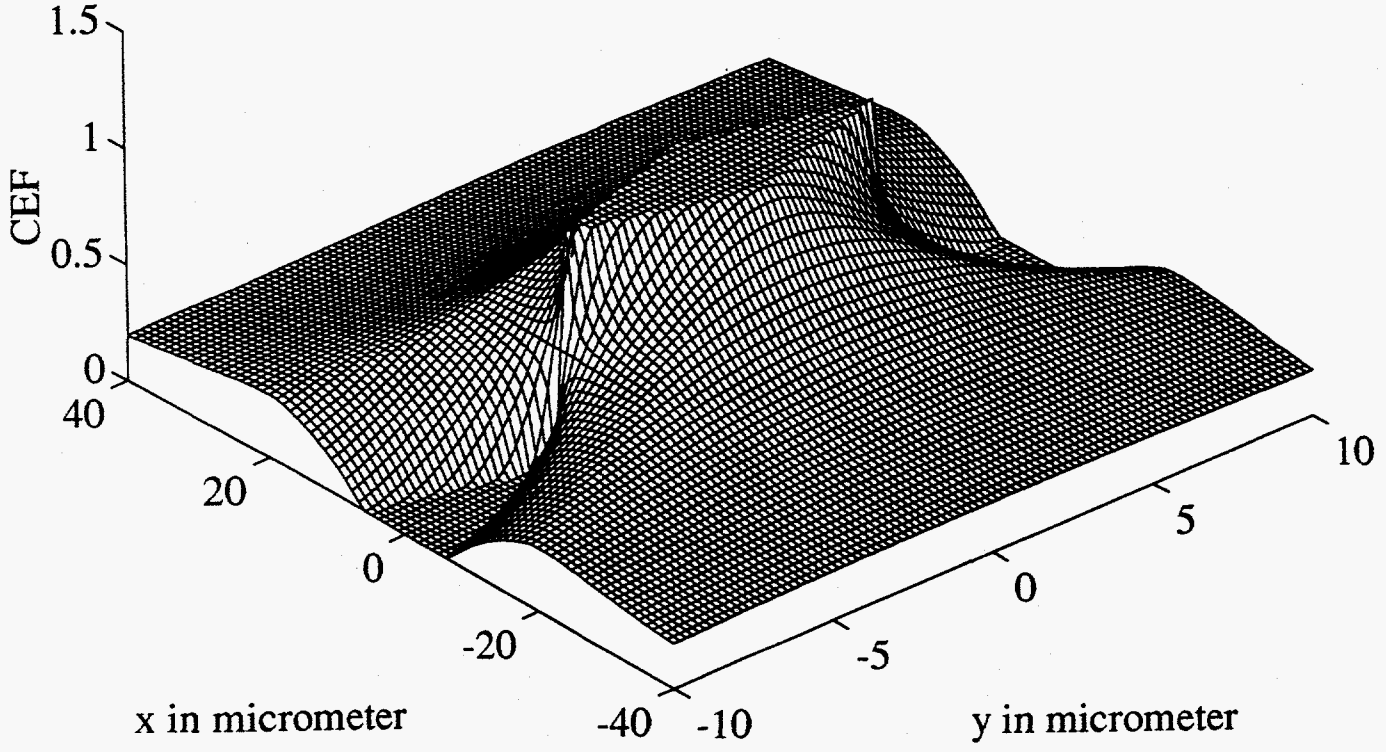
1.5
1
0.5
0
CEF
40
20
0
-20
-40
x in micrometer
-10
-5
0
5
10
y in micrometer

Fig. 3

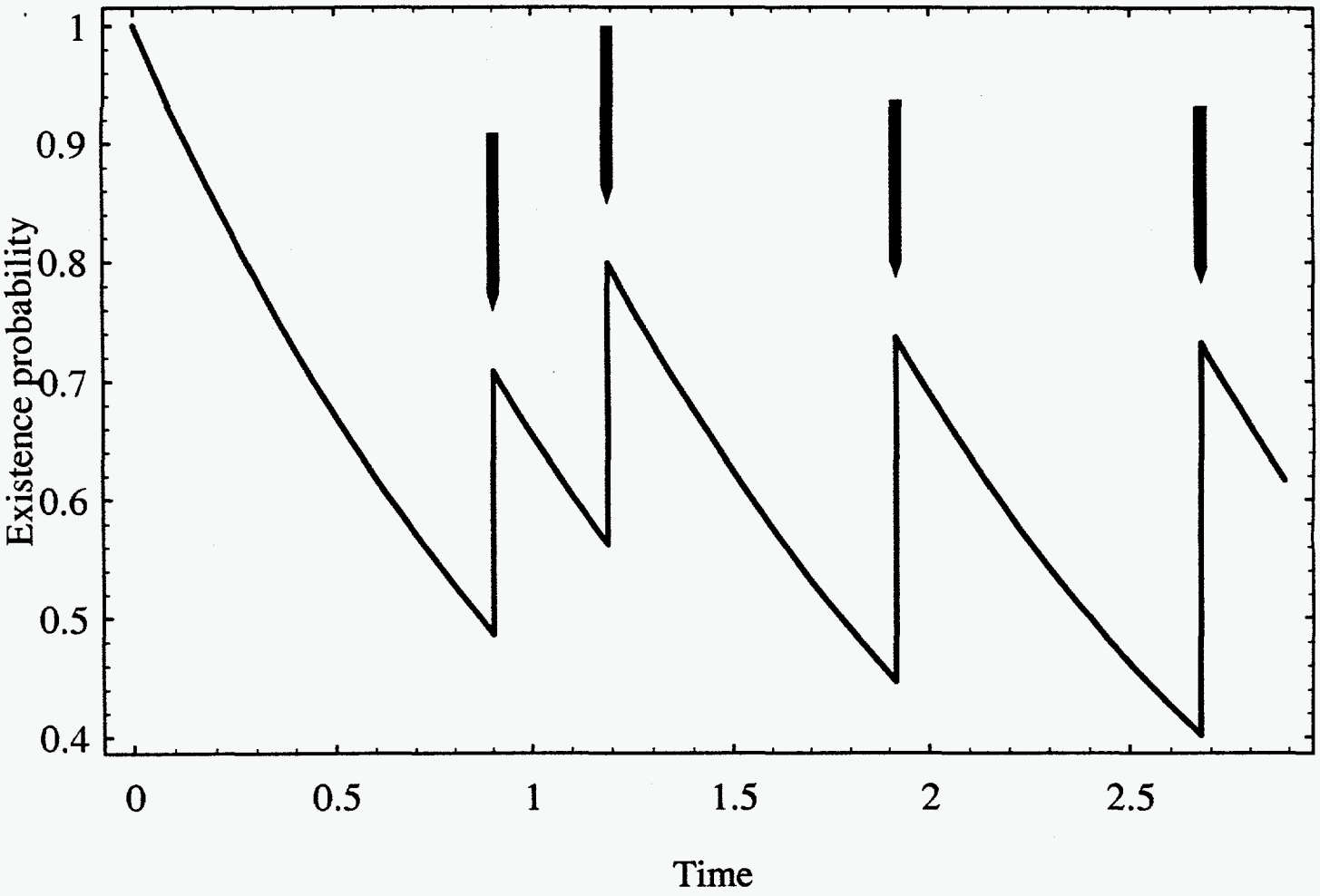

Fig. 4

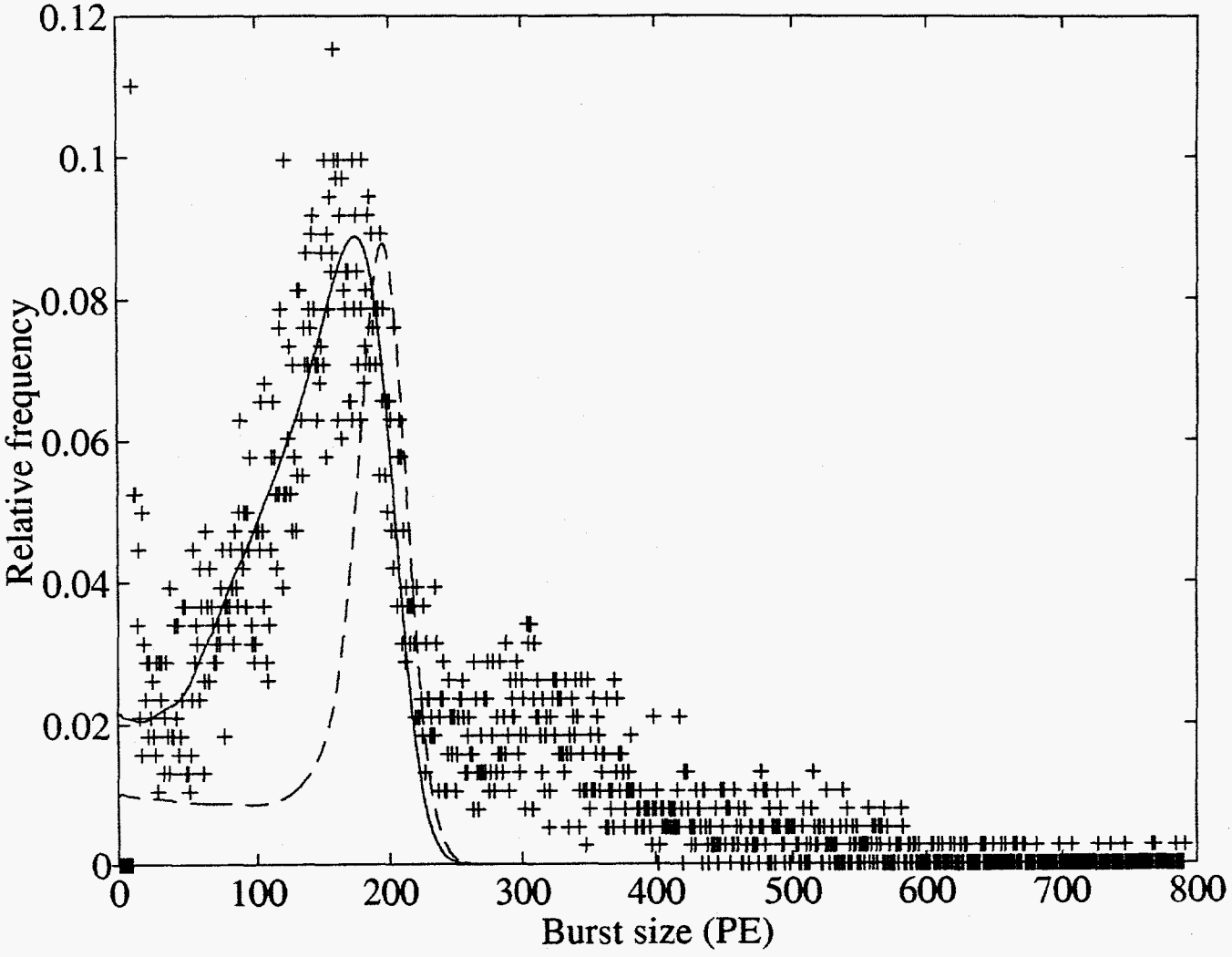
0.12
0.1
0.08
0.06
0.04
0.02
0
Relative frequency
0
100
200
300
400
500
600
700
800
Burst size (PE)

Fig. 5

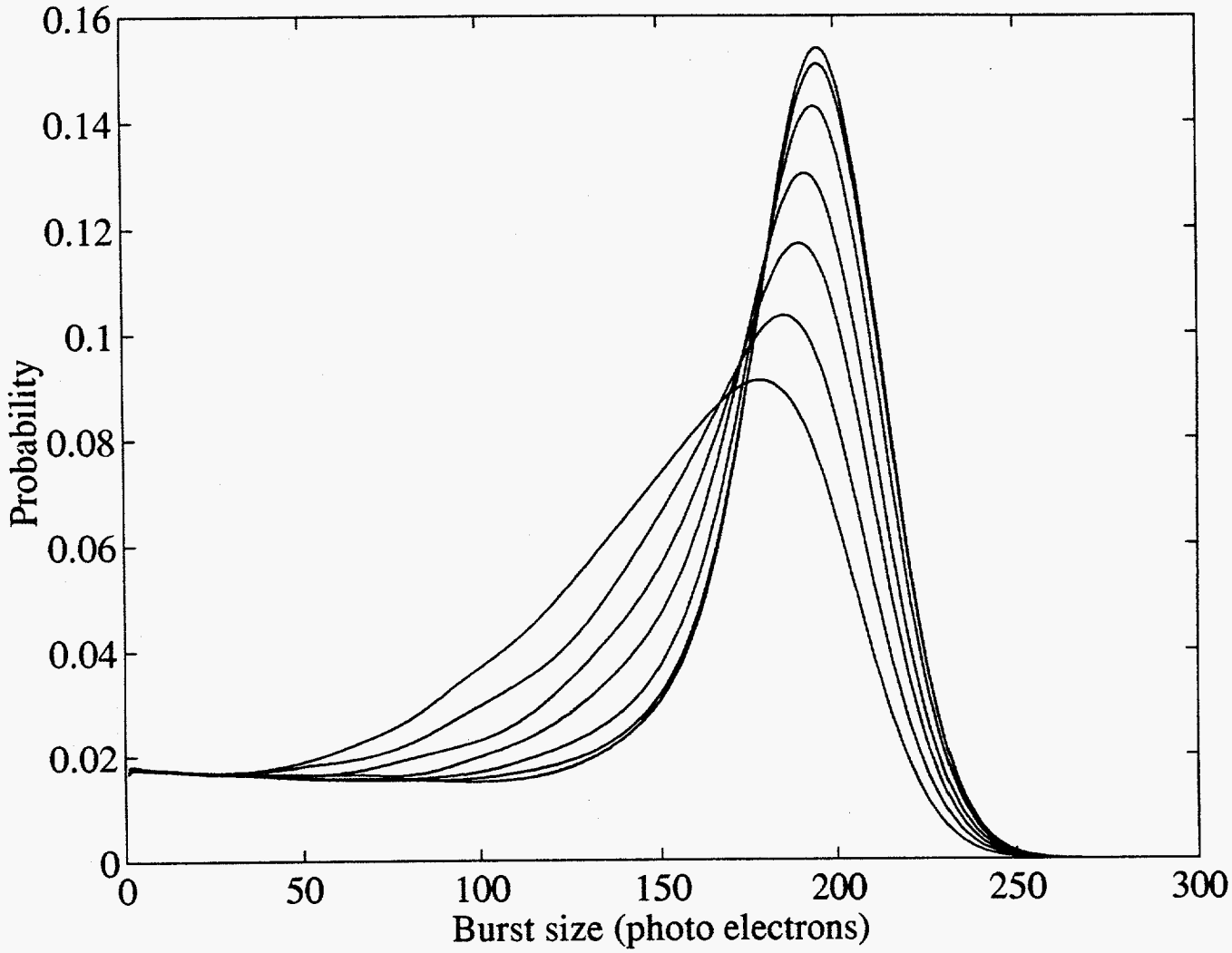
0.16
0.14
0.12
0.1
0.08
0.06
0.04
0.02
0
Probability
0
50
100
150
200
250
300
Burst size (photo electrons)

Fig. 6

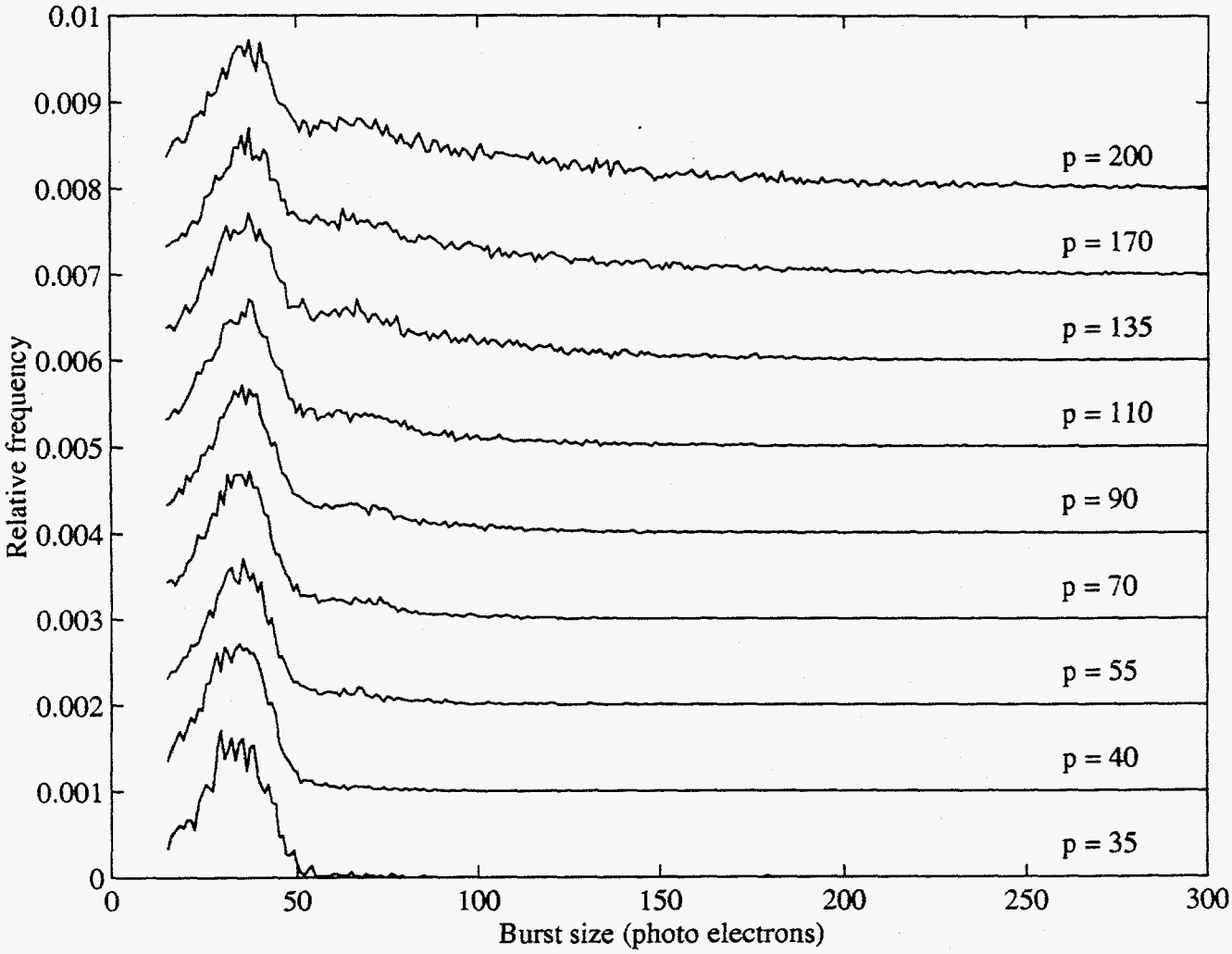
0.01
0.009
0.008
0.007
0.006
0.005
0.004
0.003
0.002
0.001
0
Relative frequency
p = 200
p = 170
p = 135
p = 110
p = 90
p = 70
p = 55
p = 40
p = 35
0
50
100
150
200
250
300
Burst size (photo electrons)

Fig. 7

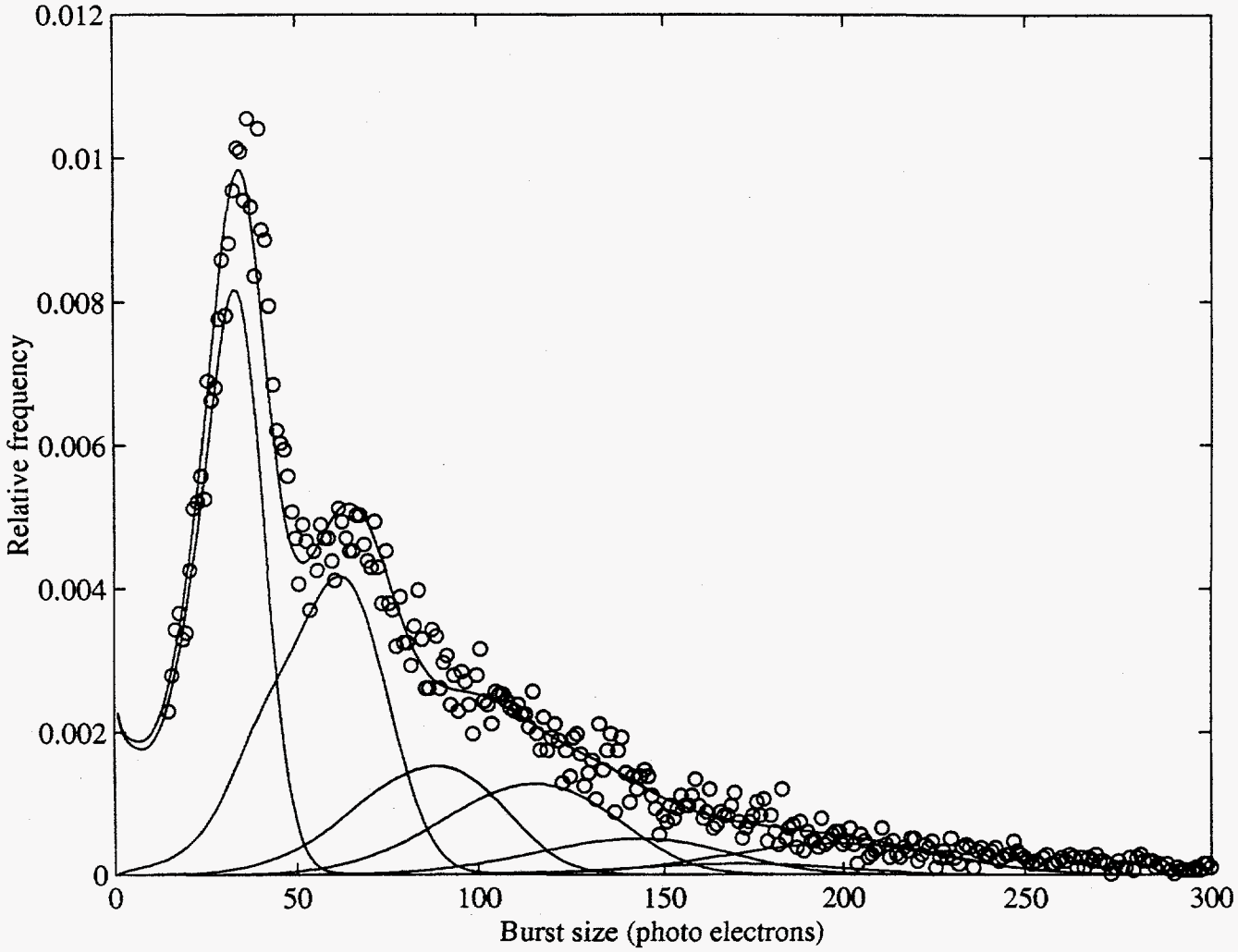
0.012
0.01
0.008
0.006
0.004
0.002
0
Relative frequency
0
50
100
150
200
250
300
Burst size (photo electrons)

Fig.8

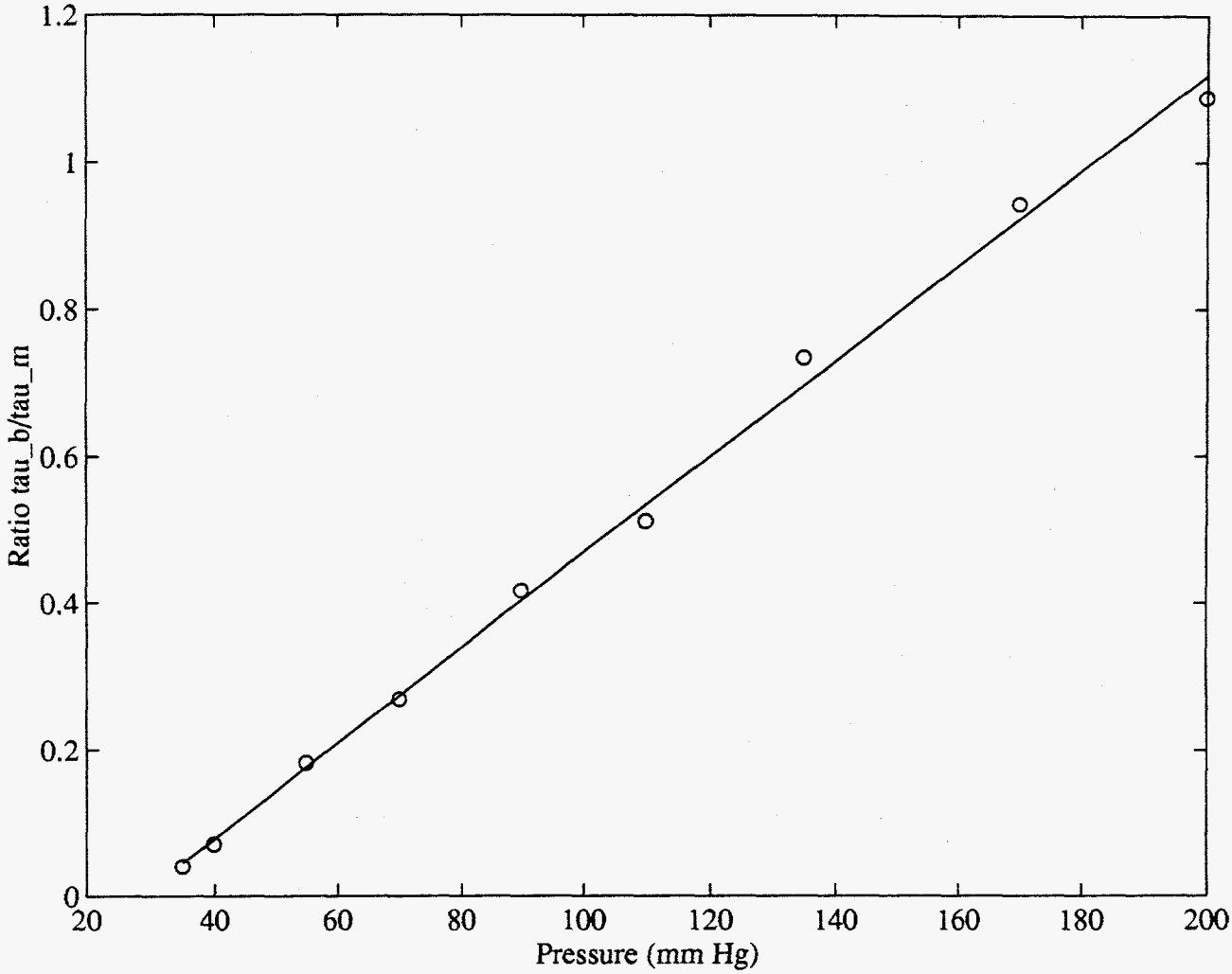
1.2
1
0.8
0.6
0.4
0.2
0
Ratio tau_b/tau_m
20
40
60
80
100
120
140
160
180
200
Pressure (mm Hg)

Fig. 9